J. Neural Eng. **5** (2008) 85–98 doi:10.1088/1741-2560/5/1/009

Non-parametric early seizure detection in an animal model of temporal lobe epilepsy

Sachin S Talathi[1,2,3], Dong-Uk Hwang[1], Mark L Spano[4], Jennifer Simonotto[5], Michael D Furman[6], Stephen M Myers[1,2,3], Jason T Winters[1,2,3], William L Ditto[1,2,3] and Paul R Carney[1,2,3,7,8,9]

[1] J Crayton Pruitt Family Department of Biomedical Engineering, University of Florida, FL 32611, USA
[2] Wilder Epilepsy Research Center, University of Florida, FL 32611, USA
[3] McKnight Brain Institute, University of Florida, FL 32611, USA
[4] NSWC, Carderock Laboratory, W Bethesda, MD 20817, USA
[5] School of Computing Science and Institute of Neuroscience, Newcastle University, Newcastle upon Tyne NE1 7RU, UK
[6] Signal Processing and Communications Laboratory, Department of Engineering, University of Cambridge, USA
[7] Department of Pediatrics, University of Florida, FL 32611, USA
[8] Department of Neuroscience, University of Florida, FL 32611, USA
[9] Department of Neurology, University of Florida, FL 32611, USA

E-mail: stalathi@bme.ufl.edu

Received 28 November 2007
Accepted for publication 5 February 2008
Published 27 February 2008
Online at stacks.iop.org/JNE/5/85

Abstract
The performance of five non-parametric, univariate seizure detection schemes (embedding delay, Hurst scale, wavelet scale, nonlinear autocorrelation and variance energy) were evaluated as a function of the sampling rate of EEG recordings, the electrode types used for EEG acquisition, and the spatial location of the EEG electrodes in order to determine the applicability of the measures in real-time closed-loop seizure intervention. The criteria chosen for evaluating the performance were high statistical robustness (as determined through the sensitivity and the specificity of a given measure in detecting a seizure) and the lag in seizure detection with respect to the seizure onset time (as determined by visual inspection of the EEG signal by a trained epileptologist). An optimality index was designed to evaluate the overall performance of each measure. For the EEG data recorded with microwire electrode array at a sampling rate of 12 kHz, the wavelet scale measure exhibited better overall performance in terms of its ability to detect a seizure with high optimality index value and high statistics in terms of sensitivity and specificity.

(Some figures in this article are in colour only in the electronic version)

1. Introduction

Epilepsy is an episodic brain dysfunction characterized by recurrent, seemingly unpredictable, spontaneous seizures [22]. The occurrence of seizures in patients without any forewarning is the most debilitating aspect of the disease. A great deal of scientific research has therefore focused on developing methods for anticipating and/or detecting seizures early enough [14] to facilitate timely therapeutic intervention, with a consequent improvement in the quality of life of the epileptic patient. The goal of seizure prediction or detection is the development of a system that not only forewarns of a seizure but also employ measures to prevent it.

Seizure anticipation algorithms can be broadly classified into two categories depending on the time horizon of the forecast: (a) seizure *prediction* algorithms that aim to detect the preictal state in the EEG minutes to hours in advance of an impending seizure [6, 7, 11–13, 19] and (b) early seizure *detection* algorithms that use EEG data to identify seizure onset, typically a few seconds in advance of the onset of

observed behavioral changes or during the period of early clinical manifestation of focal motor changes or loss of patient awareness [16, 15, 20].

A survey of the seizure prediction tools [14] suggests that many of the existing seizure prediction algorithms have not been subject to a sufficiently rigorous statistical evaluation in terms of their sensitivity (S) and specificity (K) to warrant a closed-loop seizure prevention study. The authors suggest that in order to advance toward a clinical application, future studies on seizure prediction should place a strong emphasis on sound methodology and include rigorous statistical validation. It is however important to note that the absence of sound methodology in the development of a robust seizure prediction algorithm verified over an out-of-sample, prospective, randomized test data sets, is intrinsically linked to the inherent variability of EEG data recorded from epileptic patients. Possible reasons for such high variability are the confounding effects of epilepsy types and severity in patients, the pathology of the disease, the effects of anticonvulsant drug treatments, the recording sites used, and the overall patient care environment. Animal models of epilepsy that emulate the human epileptic condition provide an opportunity to generate EEG data under controlled experimental conditions, thereby minimizing the effect of confounding variables that affect the performance of seizure prediction algorithms. An additional benefit for the use of animal models is that sufficiently large EEG data sets from recordings over several weeks can be obtained so that it is feasible to study the evolution of the disease over a longer period of time. In the case of humans, EEG data are typically obtained during the pre-surgical assessment of the patient and the duration is usually less than 10 days. The EEG data generated from these animal models can thus be a test-bed for evaluating the performance of any given seizure prediction algorithm.

The statistical robustness of early seizure detection schemes, on the other hand, [16, 18, 20] makes them more attractive for use in the development of a real-time closed-loop seizure intervention program (RCLSIP) [15]. The success of these early seizure detection methods in RCLSIPs critically depends on the time available between detection of seizure onset and clinical manifestation of the seizure through overt seizure behavior. Most seizure detection and prediction methods are based on macroscopic descriptors of low-sampled EEG (i.e. sampling rate of 200–250 Hz) which is the standard in most EEG clinical laboratories. We hypothesize that additional information about seizure generation and thus the time of seizure detection by a given early seizure detection algorithm can be enhanced through a better EEG acquisition method, through data acquired at higher sampling rate using high resolution microwire (50 μ) electrode arrays. In order to evaluate the above hypothesis, we performed a comparative study on five known univariate nonparametric dynamical measures (M) for seizure detection in terms of their ability to detect seizure onset with high statistical robustness as a function of the method of EEG acquisition. In particular we use EEG data from a rat model of chronic limbic epilepsy (CLE) using a 32-channel microwire-electrode (50 μ) array at a high sampling rate of 12 kHz as well as EEG data obtained using stainless-steel screw recording electrodes (0.8 mm) sampled at 200 Hz.

We examined five different methods M: (1) embedding delay (ED); (2) wavelet scale (WS); (3) Hurst scale (HS); (4) nonlinear autocorrelation (NLA); and (5) variance energy (VE). The rationale for the choice of M was based on the fact that each measure is non-parametric, that each tries to extract some form of correlation from the EEG data, and that the published literature on the algorithms that extract correlations in the EEG data in order to detect seizures provides meaningful results in human seizure data analysis.

The first method for seizure detection, embedding delay (ED) is motivated from encouraging results obtained through earlier works on the use of short-term Lyapunov exponent (STLE) [7–9 24], to identify preictal changes in the EEG data. Embedding delay is one of the key parameters required in the estimation of the STLE measure [1]. ED is a non-parametric measure that essentially captures critical information on the short-term correlation in the EEG data. This information can be utilized for early seizure detection. The wavelet transform (WT) based estimates have also been successfully applied by a number of groups [15, 16, 20] for seizure detection and determination of seizure onset time. The WT can be considered as an extension to the classic Fourier transform: instead of working on a single scale (time or frequency), it works on a multi-scale basis. The basic idea is to analyze the signal $x(t)$ at different frequency bands with different resolutions in order to extract correlations in the data as function of the frequency content of the signal.

Recently, [26] examined the scaling properties in the EEG data through fractal spectral estimates in order to extract signatures of an impending seizure during the preictal state. Emergent long-range correlations (fractal patterns) in the EEG data were characterized using a Hurst exponent, which is a classical measure used to determine long-range fractal content or the degree of 'roughness' in the signal. Also recently a robust seizure detection algorithm, designed primarily for the purpose of screening for seizures in long-term EEG recordings, was developed by White *et al* [25] to extract nonlinear correlations in the EEG data for seizure detection with very high statistical accuracy. The goal was to use information embedded in the seizure epoch of the EEG data to mark the location of the seizure in order to facilitate the screening of the EEG data to identify seizures in an experimental paradigm of long-term EEG data acquisition. Whether this measure can be used in an early seizure detection paradigm, wherein information in the seizure epoch is not available, remains to be tested. Finally an energy-based measure characterizing the variance in the EEG data [12] is used in this study since it is known to be the most computationally efficient measure that is sensitive to the EEG waveforms associated with seizures.

The paper is organized as follows: in section 2, we first describe the experimental procedure for preparing the CLE rat model and the method of EEG data acquisition. We then present the mathematical details on the five univariate measures used in this paper. We then describe the statistical approach used to determine the sensitivity and specificity for each measure. We develop an empirical optimality index

measure O, which allows us to have an unbiased evaluation criteria for the performance of the various measures for seizure detection. In section 3, we demonstrate various EEG seizure morphologies (EEG seizure refers to the seizure epoch observed in the recorded EEG time series data) and the common features shared by each EEG seizure. We then present results on the performance by each measure in terms of its ability to detect a seizure close to its onset time and its optimality index, encompassing the statistics on sensitivity and specificity. The overall results for the performance of each measure for a given EEG acquisition method are summarized in table 3. All the data analyzed in this work and the Matlab m-files are available from the author (SST) upon request.

2. Materials and methods

2.1. Experimental procedure for developing a rat model for chronic limbic epilepsy

2.1.1. Animals. Experiments were performed on 2 month old male Sprague Dawley rats ($n = 9$) weighing 210–265 g. All protocols and procedures were approved by the Institutional Animal Care and Use Committee of the University of Florida.

2.1.2. Surgery and electrode implantation. The top of the head was shaved and chemically sterilized with iodine and alcohol. The skull was exposed by a mid-sagittal incision that began between the eyes and extended caudally to the level of the ears to expose the bregma and lambdoidal suture. A peroxide wash was applied to the skull to remove excess soft tissue.

In six of the nine rats, a hole was drilled to insert a bipolar twist stainless-steel Teflon coated electrode (AP $-$ 5.3 mm, lateral 4.9 mm, vertical -5 mm below the dura) in the right ventral hippocampus for stimulating the rat into self-sustaining *status epilepticus*. The rat induced into *status* through electrical stimulation will develop chronic limbic epilepsy (CLE) and seize spontaneously in about 2–4 weeks [21]. Two 0.8 mm stainless-steel screw recording electrodes (Small Parts, Miami Lakes, FL) were also placed in the skull over the bilateral frontal cortices (AP 3.2 mm, lateral ± 2 mm). Two additional recording screw electrodes were placed over the parietal cortex (AP $-$ 5.3 mm, lateral $\pm$ 3.9 mm). Electrodes were labeled according to their relative positions on the rat's skulls as an LF/RF channel (left/right frontal cortex) and an LH/RH channel (left/right hippocampus). A reference screw electrode was placed on the midline 2 mm caudal to lambda and a ground screw electrode was placed just rostral to bregma (AP 2 mm, lateral 1 mm). Electrode pins were positioned in a plastic strip connector and the entire headset was glued into place using cranioplast cement (Plastics One, Inc., Roanoke, VA). In three of the nine rats, sixteen microwire recording electrodes (50 μm polyimide insulated tungsten microwires) were implanted to the left of the midline suture in a horizontal fashion in the CA1, CA2, CA3 and the dentate gyrus regions of the hippocampus. The orientation of these microelectrodes was such that the furthest left microwire was positioned at 4.4 mm caudal to bregma, 4.6 mm to the left of midline suture, and at a depth of 3.1 mm from the dura. A second array of 16 microelectrodes was placed to the right of the midline in diagonal fashion. The orientation of these microelectrodes was such that the furthest right microwire was positioned at 3.2 mm caudal to bregma, 2.2 mm to the right of midline. The closest right microwire was positioned at 5.2 mm caudal to bregma, 1.7 mm to the right of the midline suture, and at a depth of 3.1 mm from the dura. The microelectrodes were configured in four bundles (four microelectrodes in each bundle) arranged in a rectangular pattern to conform to the morphology of the hippocampus. On the long axis of the bundle each microelectrode was separated by 250 μm and, on the short axis, the separation was 500 μm. In addition, these rats also contained one bipolar, twisted, Teflon-coated, stainless-steel electrode of 330 μm diameter implanted in the right posterior ventral hippocampus (5.3 mm caudal to bregma, 4.9 mm to the right of midline suture, and at a depth of 5 mm from the dura) for stimulating the rat into self-sustaining *status epilepticus*. Four 0.8 mm stainless-steel screws were placed in the skull to anchor the acrylic headset: two screws were AP 2 mm and bilaterally 2 mm and served as the ground electrodes while two screws were AP 2 mm to the lambdoidal suture and bilaterally 2 mm and served as the reference electrodes. All the electrodes were permanently secured with cranioplast cement. Following surgery, animals were allowed to recover for one week prior to additional procedures. All the electrode placements were verified using *ex vivo* brain MRI and post-mortem histology [21].

In figure 1, we show a schematic diagram for the layout of the electrodes for the two configurations described above. For CLE rats with microwire electrodes (Micro Rat), we report results from four locations, which correspond to averaged results from channels, Ipsi-CA $\equiv$ 1, 2, 15, 16, corresponding roughly to the CA region on the ipsilateral (side with the stimulating electrodes) hippocampus, Ipsi-DG $\equiv$ 7, 8, 9, 10, corresponding roughly to the ipsilateral dentate gyrus, Contra-DG $\equiv$ 17, 18, 31, 32 corresponding to contralateral dentate gyrus region, and finally Contra-CA $\equiv$ 23, 24, 25, 26 corresponding roughly to the contralateral CA region. For CLE rats with stainless-steel screw recording electrodes (Macro Rat) we report results from the RH channel.

2.1.3. Induction of status epilepticus. All animals were electrically stimulated one week after surgery to induce *status epilepticus*. During electrical stimulation and EEG acquisition, animals were housed in specially made chambers (Bertram *et al* 1997). Biphasic square wave stimulus trains at a frequency of 50 Hz and with a pulse duration of 1 ms and intensities of 300–400 mA were continuously delivered for 50–70 min with a duty cycle of 10 s on/2 s off. During the stimulus the usual behavioral response of the animal was the display of 'wet dog shakes' and increased exploratory activity. After approximately 20–30 min of stimulation, convulsive seizures in the form of 'wet dog shakes' (up to 1 min in duration) were usually observed about every 10 min. At the end of the stimulus period, continuous EEG recordings were observed for

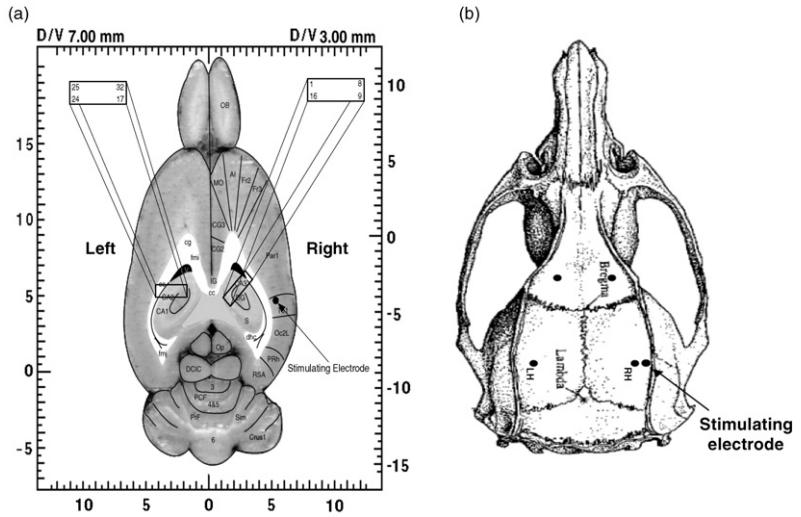

Figure 1. (a) Schematic of the layout of the microwire electrode array for EEG recordings in the CLE rat model for temporal lobe epilepsy. We show a horizontal section of the rat brain at 3 mm from the cortical surface, the depth at which the microwire array is placed in an orientation described in section 2. (b) Schematic of the placement of the stainless-steel screw electrodes in the skull for EEG recordings in the CLE rat model for temporal lobe epilepsy. We show a horizontal view of the skull of the rat and mark the location of all the recording screw electrodes as described in section 2 (LH: left hippocampus, RH: right hippocampus).

evidence of slow waves in all recorded channels. If slow waves were not demonstrated, then the stimulus was re-applied for 10 min intervals for one to three more times until continuous slow waves appeared following termination of the stimulus. Lack of response to this stimulation protocol was infrequent (<10% of animals) and was attributed in part to inaccurate placement of the stimulating electrode in the ventral hippocampus. Upon termination of continuous hippocampal stimulation, the EEG continued to demonstrate activity below 5 Hz for 12–24 h and intermittent spontaneous 30–60 s electrographic seizures for 2–4 h. Animals were observed for seizure activity and adequate food and water intake for 12–24 h after stimulation. Following behavioral stabilization, animals were returned to the vivarium for 6 to 8 weeks, during which time spontaneous seizures developed.

2.1.4. EEG/video acquisition. Following the induction of limbic status epilepticus, the rats were moved to cages that allow full mobility of the animals, good visualization for video monitoring, and a stable recording environment. Each rat cage was a 10 inch diameter cast acrylic tube which was 12 inches high with a plastic mesh floor. The rat cages were housed in a controlled environment (21 °C; humidity 60%, and standard 12 h light-dark cycle). The six Macro Rats with stainless-steel screw recording electrodes were connected by a six-channel commutator and a shielded cable to the recording system consisting of an analog amplifier (Grass Telefactor-Model 10), a 12 bit A/D converter (National Instruments, Inc.), and recording software (HARMONIE 5.2, Stellate Inc., Montreal) where each channel was sampled at a uniform rate of 200 Hz and filtered using analog high- and low-pass filters at cutoff frequencies of 0.1 Hz and 70 Hz, respectively. The three Micro Rats were connected to a 32-channel commutator, the output of which was fed into the recording system comprised of two 16-channel pre-amps (Tucker Davis Technologies), where the signals are digitized with a 16-bit A/D converter at 12 kHz, and sent over a fiber optic cable to a Pentusa RX-5 DSP board (Tucker Davis Technologies), where they are bandpass filtered between 1.5 Hz and 7.5 kHz. In-house software was used to store the data acquired from the Pentusa system in a 16-bit binary format for later processing. Both recording units were synchronized to a video unit for time-locked monitoring of behavioral changes. The recording systems run continuously so that data sets containing ictal as well as interictal behavior could be collected for analysis.

2.1.5. Data characteristics. Long-term continuous EEG recordings of the three Micro Rats used for recordings yielded a total of 22 seizures, while the six Macro Rats yielded a total of 16 seizures. Seizures were identified by review of technician logs and visual inspection of all recordings. Seizures were confirmed and classified by a board-certified epileptologist and experimental neurologist (PRC) and vetenerary neuroscientist (Dr Wendy Norman), who made an independent determination of the time and anatomical location of electrographic seizure onsets. These seizures were used to analyze the performance of each of the five different seizure detection schemes, *M*.

2.1.6. Measures for seizure detection. All the measures *M* for seizure detection are applied to the following data sets.

(1) *Micro Rat at 12 kHz (12K).* One hour of EEG data from 32 channels around each of the 22 seizures observed and 50 randomly selected one hour inter-ictal data sets from all the 32 channels for each of the three rats.
(2) *Micro Rat at 200 Hz (200-I).* The same data set as above, down-sampled to 200 Hz. The downsampling to 200 Hz was done for comparative study with data recorded using stainless-steel electrodes at 200 Hz.

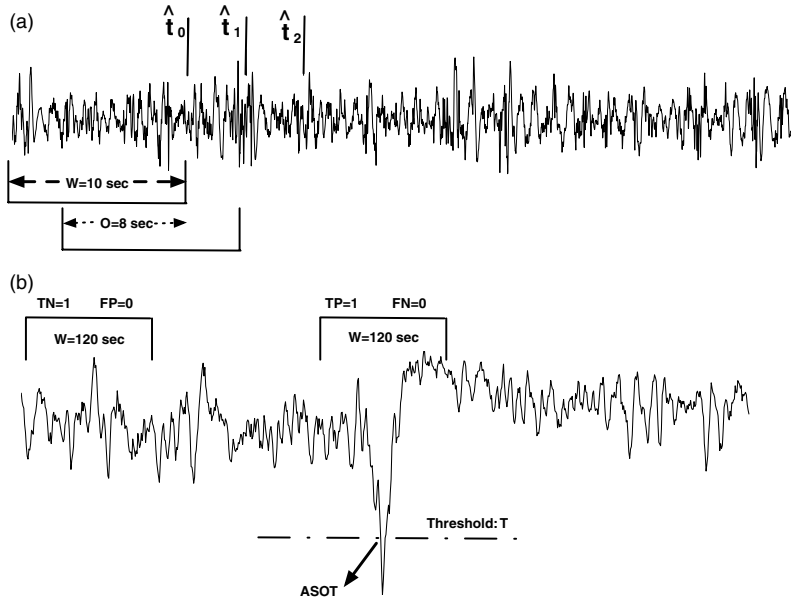

Figure 2. (a) By windowing raw EEG data and producing seizure detection estimates (M) at the end of each window indicated at times $\hat{t}_0, \hat{t}_1$ and $\hat{t}_2$, a typical result (b) is generated and analyzed for the purpose of generating the statistical estimates for sensitivity (S) and specificity (K). Here ASOT is the algorithmic seizure onset time indicated by the threshold T, with TN: true positive; FP: false positive; TP: true positive; and FN: false negative.

(3) *Macro Rat at 200 Hz (200-M).* One hour EEG data from a single channel (RH channel) around each of the 16 seizures observed and 50 randomly selected one hour interictal data sets from the same channel for each of the six rats.

For each of the 1 h data sets, as shown in figure 2(a), we consider a moving window of 10 s duration with 8 s overlap between consecutive windows to determine the value of a given measure M in that window. Note that the time stamp $\hat{t}$ for M is the end time of the 10 s window under consideration, corresponding to a prospective evaluation of each measure M (figure 2(a)). Let $x(t)$ denote the EEG data in a given 10 s window. The dynamical measures $M(\hat{t})$ are computed from $x(t)$ as follows:

- *Embedding delay (ED)*: we define the embedding delay

$$\tau = \min(\tau_1, \tau_2) \tag{1}$$

τ_1 is the first minimum of average mutual information, $I(T)$, defined by [1]

$$I(T) = \sum_{x(t),x(t+T)} P(x(t), x(t+T)) \log_2 \times \left[\frac{P(x(t), x(t+T))}{P(x(t)) \cdot P(x(t+T))}\right]$$

where $P(x(t), x(t+T))$ is the joint probability density for the EEG data having values $x(t)$ and $x(t+T)$ respectively, while $P(x(t))$ and $P(x(t+T))$ are individual probability densities for the EEG data to have values $x(t)$ or $x(t+T)$ respectively.

τ_2 is obtained as the first zero crossing of the autocorrelation function C defined by

$$C(T) = \sum_t [x(t) - \bar{x}][x(t+T) - \bar{x}]$$

with

$$\bar{x} = \frac{1}{T}\sum_{t=0}^{T} x(t)$$

- *Wavelet scale (WS)*: the wavelet scaling ζ is computed as follows—we use a sombrerro mother wavelet [10],

$$\psi(t) = \frac{1}{\sqrt{2\pi}}(1 - t^2)\, \mathrm{e}^{\frac{-t^2}{2}}$$

to compute the continuous wavelet transform of time series $x(t)$ as

$$W(\tau, s) = \int x(t) \frac{\psi\left(\frac{t-\tau}{s}\right)}{\sqrt{s}} \mathrm{d}t.$$

The normalized wavelet energy is then obtained from

$$\tilde{W}(\tau, s) = \sqrt{\frac{W^2(\tau, s)}{\sigma^2}}$$

where σ^2 is the sample variance of the data set $\{x(t)\}$. The wavelet scaling function ζ is then given by

$$\zeta = \mathrm{argmax}_s \left(\sum_\tau \tilde{W}(\tau, s)\right); \tag{2}$$

- *Hurst scale (HS)*: we use trend-corrected rescaled-range analysis [2] to determine the Hurst scaling α as follows. Let

$$\bar{x}_\tau = \frac{1}{\tau}\sum_{t=0}^{\tau} x(t).$$

For a given τ we define the deviation from the sample mean at any given time t as $\bar{e}_t = x(t) - \bar{x}_\tau$. The cumulative sum of the deviations is then given by $X(t_0, \tau) = \sum_{t=1}^{\tau} \bar{e}_{t_0+t}$. The trend-corrected range of the data is then given by

$$R(t_0, \tau) = \max(X(t_0, \tau)) - \min(X(t_0, \tau))$$

for the range $1 < t_0 \leqslant \tau$. If $S^2(t_0, \tau)$ represents the sample variance of the data set $\{\bar{e}_{t_0+i}\}_{i=1}^{\tau}$, the rescaled range is then given by

$$R(\tau) = \left\langle \frac{R(t_0, \tau)}{S(t_0, \tau)} \right\rangle_{t_0}.$$

Assuming a power-law scaling for the rescaled range function $R(\tau)$, i.e., $\log(R(\tau)) = \beta \log(\tau) + \log(\alpha)$, we obtain the Hurst scaling α as

$$\alpha = \frac{R(\tau)}{\tau^\beta}; \tag{3}$$

- *Nonlinear autocorrelation (NLA)*: we define the nonlinear autocorrelation ω based on the algorithm for seizure detection reported in [25] as follows. The EEG data $x(t)$ in a given moving window of 10 s duration are divided into two sub-bands each of 5 s in duration. For the data in each sub-band, we compute the maximum and minimum over a group of $N = 5F_S/100$ points, denoted by $\{S_i\}|_{i=1}^{100}$, where F_S is the sampling rate of the EEG recordings. Following [25], we then compute the relative maximum (RU) and minimum (RL) for each of the 100 N-point groups, S_i, as

$$RU_i = \min[\max(S_i), \max(\max(S_{i+1}), \max(S_{i+2}))]$$

and

$$RL_i = \max[\min(S_i), \min(\min(S_{i+1}), \min(S_{i+2}))].$$

For each sub-band we then define a metric for autocorrelation given by

$$\overline{M} = \sum_{i=1}^{100} (RU_i - RL_i) \tag{4}$$

We finally compute ω as the average of the autocorrelation metric $\overline{M}$ computed over each sub-band.

- *Variance energy (VE)*: the energy content of the raw EEG data characterizing the changes in the signal strength for a given time epoch of EEG data $x(t)$ is determined through the VE as follows: the EEG data $x(t)$ of 10 s in duration are divided into five sub-segments of 2 s duration. The variance σ^2 of the difference signal for each 2 s segment of the EEG data is determined and the VE estimate is then obtained as

$$MV(t) = \frac{1}{5} \sum_{i=1}^{5} \sigma_i^2. \tag{5}$$

2.1.7. Statistical test and optimality index. The performance of each measure M for seizure detection is analyzed according to the statistical robustness of a given measure to detect a seizure event with minimal false positives and on the ability of M to detect seizure onset early enough as determined through ΔT = ASOT − ESOT. ASOT is the algorithmic seizure onset time obtained through a seizure event marked by the threshold T_M crossing of a given measure M and ESOT is the electrographic seizure onset time, as determined by visual inspection of the EEG data by a trained epileptologist. In order to determine the ASOT, we consider a seizure detection horizon of 1 min around the ESOT for each seizure considered such that the ESOT is in the center of the 2 min time window. The ASOT is determined only when an event is marked within this time window. An event marked by a given measure M, corresponding to the threshold T_M crossing outside the seizure detection horizon {ESOT − 60, ESOT + 60} s is considered to be a false positive event.

The statistical robustness of a given measure is determined through the two estimates of sensitivity (S) and specificity (K) defined through the following quantities. Event: corresponds to threshold T_M crossing of a given seizure detection measure; true positive: corresponds to a seizure event marked by M; false positive: corresponds to a non-seizure event marked by M; true negative: corresponds to non-seizure event not marked by M; and false negative: corresponds to a seizure event not marked by M.

Sensitivity and specificity are now defined as follows.

- *Sensitivity (S)* is defined as the likelihood of detecting a seizure if it is present and is given by the ratio of the number of true positive events to the sum total of the number of seizures present in the data set.
- *Specificity (K)* is defined as the likelihood of not triggering a false event detection and is given by the ratio of the number of true negative events to the sum of both true negative events as well as the number of false positives.

In figure 2(b), we demonstrate an example of the computation of S and K. For a given EEG data set (e.g., Micro Rat at 12 kHz) each 1 h EEG epoch from seizures ($N_S = 22$) and control data ($N_C = 50$) is divided into 2 min bins. It should be noted that each EEG seizure data set comprises a 2 min window consisting of a seizure epoch. Within this time window, if M triggers an event detection, we consider it a true positive (TP = 1) and a false negative (FN = 0), as shown in figure 2(b). If no event detection is triggered by M for each of the two minute time windows outside the seizure epoch time window, we consider it a false positive (FP = 0) and a true negative (TN = 1). Sensitivity S and Specificity K for a given measure M is then computed as

$$S = \frac{\sum_{i=1}^{N_s} \mathrm{TP}_i}{\sum_{i=1}^{N_s} \mathrm{TP}_i + \sum_{i=1}^{N_s} \mathrm{FN}_i} \tag{6}$$

$$K = \frac{\sum_{i=1}^{N_s} \sum_{w=1}^{29} \mathrm{TN}_i^w + \sum_{i=1}^{N_c} \sum_{w=1}^{30} \mathrm{TN}_i^w}{\sum_{i=1}^{N_s} \sum_{w=1}^{29} \mathrm{TN}_i^w + \sum_{i=1}^{N_c} \sum_{w=1}^{30} \mathrm{TN}_i^w + \sum_{i=1}^{N_s} \sum_{w=1}^{29} \mathrm{FP}_i^w + \sum_{i=1}^{N_c} \sum_{w=1}^{30} \mathrm{FP}_i^w} \tag{7}$$

Table 1. Abbreviations used in the text.

Abbreviation	Details
Macro Rat	The CLE rat implanted with stainless-steel recording electrodes
Micro Rat	The CLE rat implanted with microwire electrode array
12K	EEG data set from Micro Rat sampled at 12 kHz
200-I	EEG data set from Micro Rat down-sampled to 200 Hz
200-M	EEG data set from Macro Rat sampled at 200 Hz
RCLSIP	Real-time closed-loop seizure intervention program
ESOT	Electrographic seizure onset time
ASOT	Algorithmic seizure onset time
M	Set of seizure detection measures
ED	Embedding delay
WS	Wavelet scale
HS	Hurst scale
NLA	Nonlinear autocorrelation
VE	Variance energy

where $N_s = \{22, 16\}$ for Micro Rat and Macro Rat EEG data sets, respectively, and $N_c = 50$.

It is desirable for any seizure detection scheme considered for use in an RCLSIP to have a very high sensitivity and specificity. In order to evaluate the overall performance of a given measure M with the aim of its utility in RCLSIP, we define an optimality index measure, O, as

$$O = \frac{(S + K)}{2} - \frac{\Delta T}{\overline{D}} \tag{8}$$

where $\overline{D}$ is the mean seizure duration obtained from the seizure data set of Macro Rats ($\overline{D} = 57.9$ s) and Micro Rats ($\overline{D} = 40.55$ s) respectively. According to the definition of S, K and ΔT, O is a bounded function, $\frac{-60}{\overline{D}} \leqslant O \leqslant 1 + \frac{60}{\overline{D}}$. A higher O indicates a better overall performance of a given measure M in terms of its suitability for use in RCLSIP.

In table 1, we summarize all the abbreviations used in the text.

3. Results

3.1. Raw EEG recordings

EEG signals from long-term continuous *in vivo* recordings comprise several components: seizure activity, interictal spiking activity, artifacts, state-dependent EEG modulation and noise, making seizure detection a non-trivial task [25]. Artifacts are the component of the EEG signal not emanating from the brain, but primarily contributed by movements of the jaw muscles while chewing, scratching of the headstage, 60 Hz electrical line noise, and clipping of the EEG signal during data acquisition. State-dependent changes are evident in the EEG recordings through the presence of a variable low frequency (1–10 Hz) component in the signal corresponding to a sleep versus an awake state of the animal. In addition, deterioration of the recording electrodes in long-term recordings contributes to the varying amplitude of EEG signal recordings. In figure 3, we show an EEG segment of about 1.5 h containing a seizure and demonstrate some of the other contributions to the EEG signal from the above-mentioned sources.

In figure 4, we illustrate three examples of EEG seizures from the CLE rat model, as described in [3], with the corresponding time–frequency plot. In the first example, the EEG seizure begins with a very high amplitude spike (pop) followed by suppression of the background activity, which is followed in turn by a gradual increase in amplitude of the EEG signal, leading to a sustained high amplitude rhythmic activity during the entire seizure epoch. In example two, the EEG seizure begins with a sudden increase in amplitude of the EEG signal followed by sustained high amplitude rhythmic activity during the seizure epoch. Finally, in example three the EEG seizure begins with the suppression of background activity, which is then followed by a gradual sustained increase in EEG amplitude during the entire seizure epoch. It has been our observation that the clinical manifestation of the seizure becomes evident during the sustained high amplitude EEG activity in the seizure epoch. The observation that two of the three EEG seizure morphologies presented above have a characteristics signature of suppression of the EEG activity before any clinical manifestation of the seizure and the fact that these represent the majority of EEG seizure types that we observe in the rat CLE model motivate us to study the feasibility of detecting these seizures early enough to invoke a closed-loop seizure intervention strategy. In order to access the performance of each seizure detection method in terms of its ability to detect seizure onset, we mark the EEG seizure onset time as the first time point in the EEG seizure epoch when the amplitude of EEG signal shows a sustained increase in amplitude. This ESOT was agreed upon by the certified epileptologist in the group.

One of the key parameters in assessing the performance of different seizure detection measures in their ability to detect seizure is the time difference between the ESOT and the ASOT, $\Delta T = \text{ASOT} - \text{ESOT}$. This is one of the key parameters in the optimality index O that we use to assess the performance of the seizure detection measures presented in this work.

3.2. Threshold choice for seizure detection

An event is marked by a given measure M when it crosses a threshold T_M. ASOT is determined as the time of crossing of T_M by M. We determine an optimal threshold for each measure that maximizes $SK = \frac{S+K}{2}$. In figure 5, we show an example of the variation of SK as function of threshold T_ζ computed for the measure WS, for each EEG data set used (12K, 200-I and 200-M). We see that for the measure WS, the optimal threshold value $T_\zeta = 8.5$ for each of the EEG data sets.

In table 2, we summarize the threshold T_M used for each of the measures M when applied to the EEG data sets.

3.3. Performance analysis

In figure 6, we present a sample 5 min EEG epoch of a seizure obtained from a 200-M EEG data set. The time evolution of each of the five seizure detection measures is shown below the sample EEG trace in order to demonstrate the ability of each of measures to successfully trigger an EEG seizure event. For an appropriate choice of threshold T_M, as obtained above, each

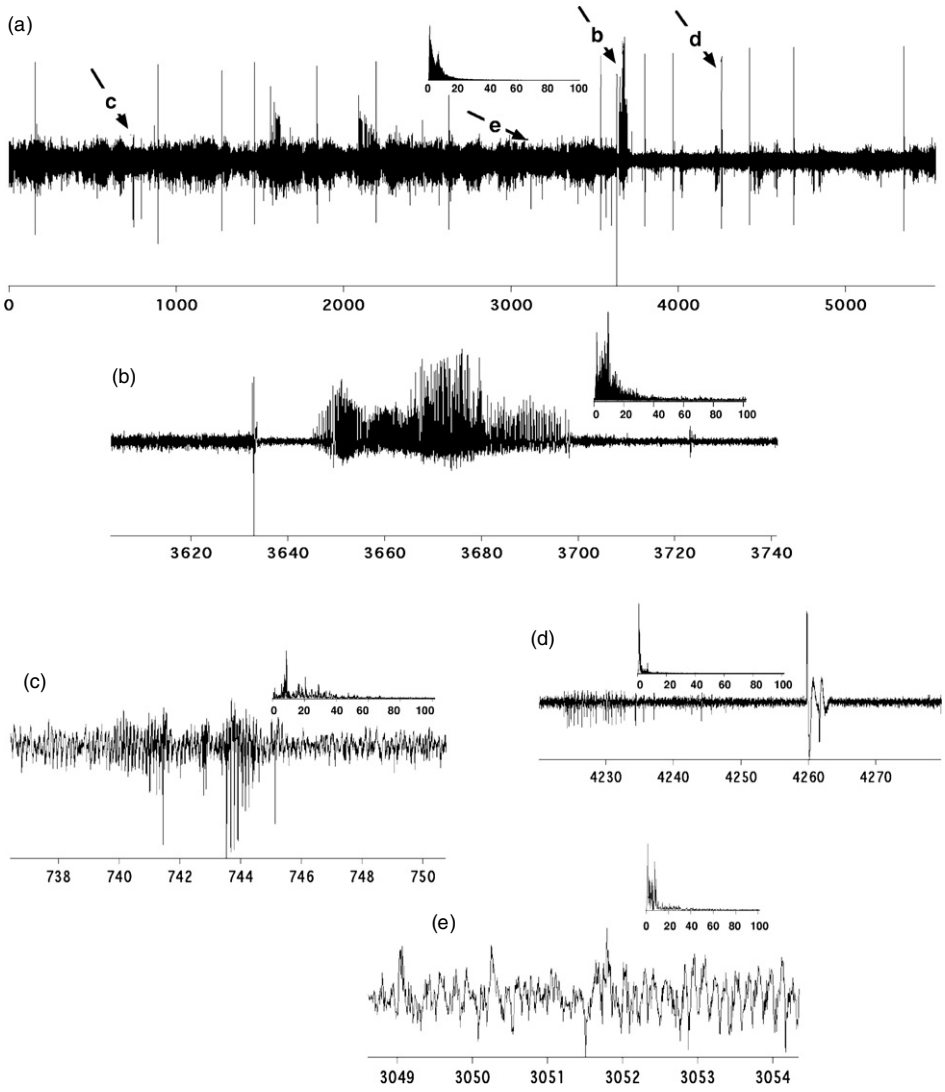

Figure 3. Raw EEG data of about 1.5 h demonstrating different components present in EEG data. (a) The entire 1.5 h epoch of EEG data and its power spectrum (inset). Various time points marked on the data correspond to different features that can be identified in the EEG. (b) A typical EEG seizure starting with a large amplitude spike, followed by suppression of the background activity and the subsequent buildup of rhythmic spiking activity. (c) An example of a typical chewing artifact present in the EEG data. (d) An example of an interictal spike in the EEG data. (e) The background activity is shown. Peaks in the delta and theta frequency band are evident, corresponding to the sleep/preconscious wake state of the rat. In all the figures above, we show the corresponding power spectrum in the inset.

Table 2. Threshold values of the dynamical measures used to mark an event. Each column in the EEG data set {12K, 200-I, 200-M} corresponds to threshold values used for the measures (ED, WS, HS, NLA, VE). The trigger direction determines the direction in which a given measure has to cross the threshold to mark an event. For example, $\uparrow$ corresponds to the value of M rising above T_M in order to mark an event. Similarly, $\downarrow$ corresponds to value of T_M falling below T_M in order to mark an event. For trigger direction with superscript σ, the actual threshold is $T_M \cdot \sigma$, where $\sigma = \text{median}\left(\frac{|M|}{0.645}\right)$.

Location	EEG Data set			Trigger Direction
	12K	200-I	200-M	
Ipsi-CA	(250.0, 8.50, 6.75, 2.00, 2.00)	(5.0, 8.5, 2.8, 1.50, 1.75)	(6.0, 8.5, 2.6, 1.5, 2.5)	
Ipsi-DG	(215.0, 10.0, 6.75, 2.00, 2.25)	(5.0, 9.0, 2.7, 1.75, 2.50)		$(\downarrow, \uparrow, \downarrow, \uparrow^{\sigma}, \uparrow^{\sigma})$
Contra-DG	(265.0, 9.00, 6.75, 2.25, 2.25)	(5.0, 9.0, 2.8, 1.25, 2.25)		
Contra-CA	(275.0, 9.00, 6.75, 1.50, 1.00)	(5.0, 10., 2.4, 1.50, 2.25)		

measure M is able to detect a seizure event, as can be seen from the figure 6.

We next perform a comparative analysis of each seizure detection measure dependent on the method of EEG

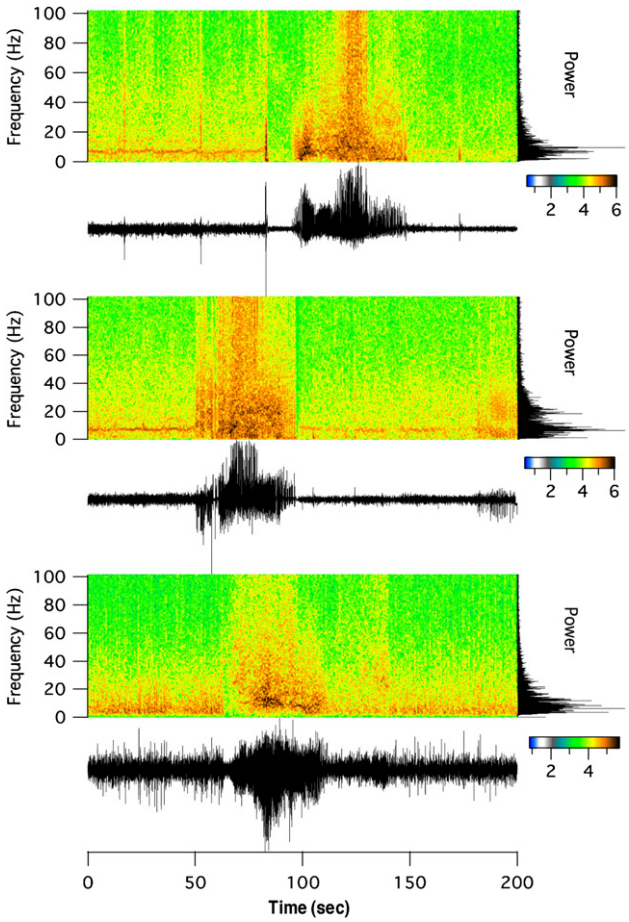

Figure 4. Examples of EEG seizure from a 200-I EEG data set of the rat model of chronic limbic epilepsy. We see that there is a sustained increase in energy in the frequency band 0–50 Hz for the entire duration of the EEG seizure.

acquisition (i.e., the electrode type, the sampling rate of the EEG acquisition and electrode placement). Each measure, M, is analyzed in terms of its ability to detect seizures as a function of delay in detection, ΔT and the optimality index, O. ΔT determines how well a given measure can detect EEG seizure close to the ESOT time. O is an overall statistical performance measure for a given seizure detection scheme that measures the ability of measure M to detect seizure with high sensitivity and specificity. In figure 7, the seizure detection measures are compared for their performance as a function of the EEG sampling rate for a given electrode location (Ipsi-lateral CA; Ipsi-lateral DG; Contra-lateral CA; Contra-lateral DG) and electrode type (microwire). For example, in figure 7-1(a) left, the bars represent the median delay ΔT in seizure detection for each of the five seizure detection measures for the case of 12 K and 200-I EEG data sets, when the EEG data were obtained using microwire electrode array located in the ipsi-lateral CA region of the rat brain. The mean delay in detection is shown along with the corresponding standard error, representing the 95% confidence interval band and represented by the blue error bars. The boxplot in figure 7-1(a) right summarizes the overall ΔT distribution for all the five seizure detection measures for the cases of 12K and 200-I EEG data sets. We see that the overall performance of all the seizure detection measures, in terms of their ability to detect seizures close to the ESOT, is better at higher EEG sampling rates for microwire electrodes located in the ipsi-lateral CA region in the brain. Also from the boxplot for the optimality index in figure 7-2(a) right, we see that for a given location, i.e., ipsi-lateral CA region, and for a given electrode type, i.e., microwire, the overall statistical performance of M is better at higher sampling rates. This suggests that correlations in the EEG seizures are better reflected by data acquired at higher sampling rates.

In figure 8, we compare the performance of M dependent on the location of the electrodes for given sampling rate (12 kHz, 200 Hz) and the electrode type (microwire). As can be seen figure 8-1(a) right, overall the performance of the five dynamical measures in terms of ΔT is the best for locations A and D, which correspond to microwire electrodes placed in the CA regions of the ipsi- and contra-lateral hippocampus. This result is particularly interesting as it sheds light on the probable origin of the seizure in the CA region in the hippocampus. A similar observation can be made from results in figure 8-1(b) right for overall ΔT in different locations at lower sampling rates of EEG acquisition.

Finally in figure 9 we present results comparing the performance of the five detection measures as function of the electrode type used for EEG recordings for a given sampling rate (200 Hz). Again as can be seen from figure 9-1(a), bottom, the overall performance of all the seizure detection measures is better in terms of ΔT for the 200-I EEG data set. Since the microwire recording electrodes are located in the hippocampus and are much closer to the source of seizure origin in the CA region, the dynamical measures M determined from the 200-I EEG data set have much higher likelihood of picking up the seizure close to the electrographic seizure onset time. The stainless-steel screw electrodes are located on the skull, in the region right above the parietal cortex and the EEG recorded on this electrode is the summation of activity over a much larger region of the brain. ΔT determined from the seizure detection measures over this low-resolution EEG data is therefore much larger than ΔT determined with the 200-I EEG data set. The optimality index is comparable in terms of the median values; however, the distribution of the O measure for each of the detection measures is skewed to the top for the 200-I measure. This indicates that the sensitivity and specificity of seizure detection for the 200-M EEG data set is better than that for the 200-I data set. One possible reason for this result is that the EEG data set for Macro Rats was low-pass filtered below 70 Hz and much of the frequency content in the EEG is restricted to a frequency band of 2–50 Hz. Thus the probability of false detection is lower.

In table 3, we summarize all the results discussed above in order to determine which measure for seizure detection is most suitable for a given EEG acquisition method. For example, we see that for a given sampling rate, location of the electrodes and electrode type, there are typically two or three better seizure detection measures, as determined by the delay in seizure detection with respect to the ESOT (ΔT), statistical robustness (SK), and the optimality index (O), which is linear

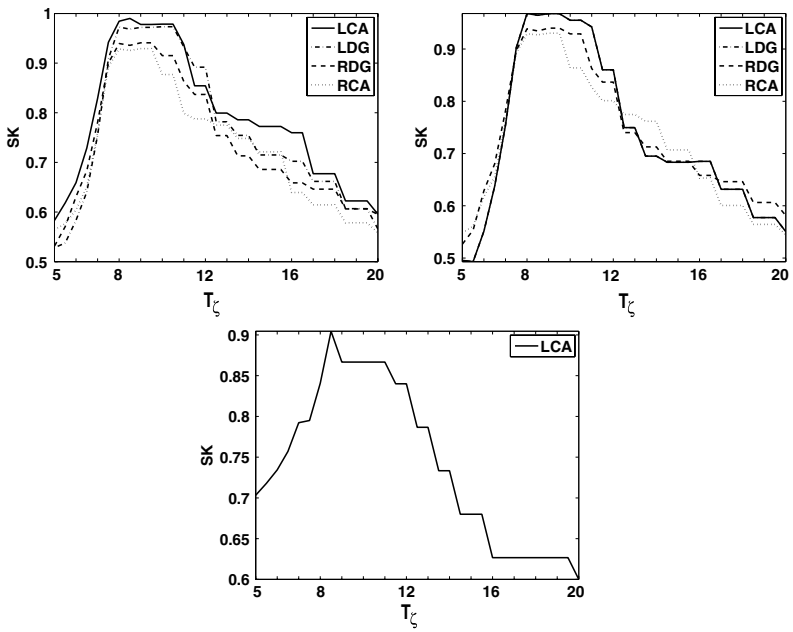

Figure 5. Example demonstrating the variation in SK measure as function of threshold T_ζ for measure WS to trigger an event detection for each of the three EEG data sets.

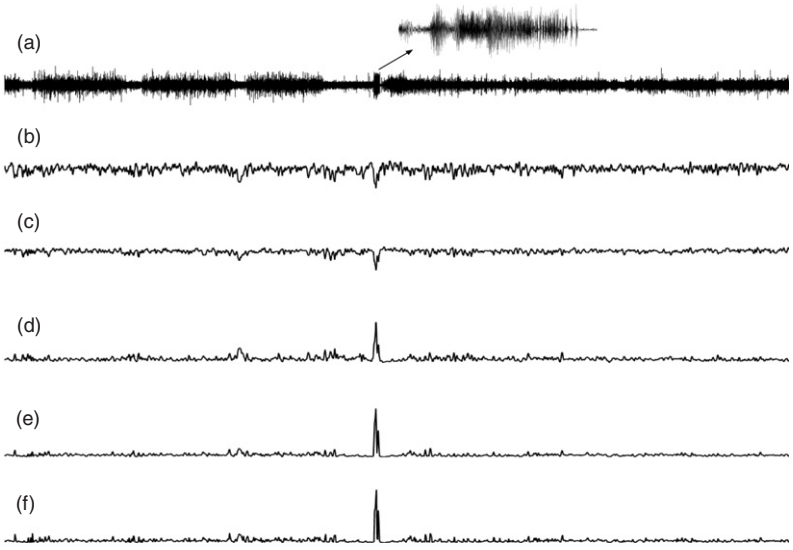

Figure 6. Example of a 5 min EEG trace from EEG data set 200-M containing a seizure and the corresponding measures, M, computed for the EEG data. The measures ED, WS, HS, NLA and VE are shown in (b)–(f), respectively.

combination of ΔT and SK. The following nomenclature was used to summarize our results in table 3: $A > B$ ($A \geqslant B$, and $A \sim B$) represents, method A is significantly better than B, i.e., greater than 10% difference in the performance measures {median(ΔT), SK, O} (greater than but not significant than B i.e., greater than 5% difference but less than 10% , similar to B, i.e., less than 5%). Overall, under the experimental conditions considered in this work, the wavelet scale measure (WS) for seizure detection had better performance than all other measures with respect to ΔT, SK and O.

4. Discussion

A number of seizure detection/prediction algorithms have been proposed over past many years [6, 7, 11–13, 15, 16, 19, 20]. A survey of the literature on seizure prediction algorithms was recently conducted by Mormann *et al* [14]. The authors suggest that many of the algorithms suggested for prediction do not perform any better than a random predictor. In addition many of these prediction schemes have not been subject to rigorous statistical validation using an out-

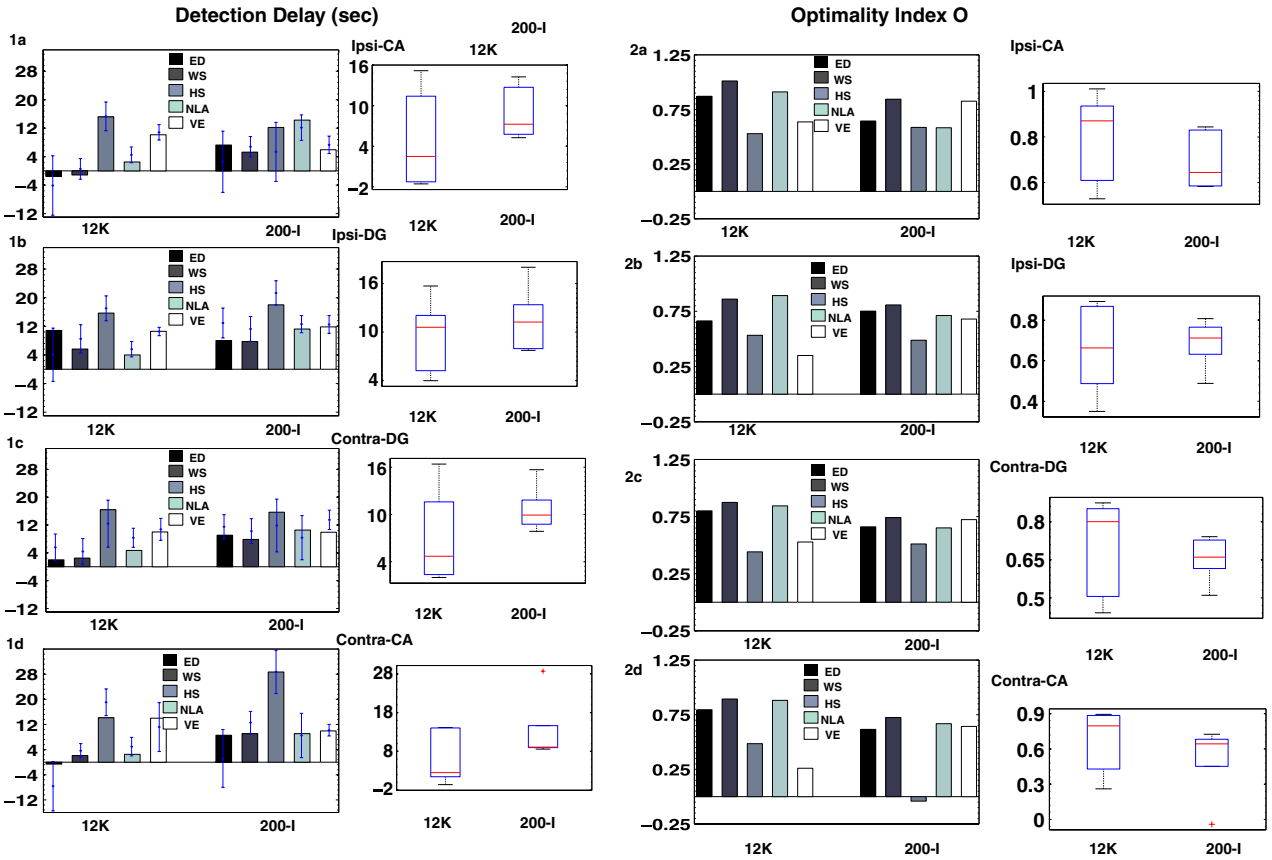

Figure 7. Comparison of performance of the seizure detection measures M, as a function of the EEG sampling rate for a given electrode placement in the brain and a given type of recording electrode. In figures 7-1(a)–(d), we compare the median delay in detection for each of the five seizure detection measures and the overall performance in terms of sampling rate (boxplot) for a given electrode placement in the brain corresponding to the following regions: ipsilateral CA, ipsilateral dentate gyrus, contralateral dentate gyrus and contralateral CA, respectively. In figures 7-2(a)–(d) a similar comparison is made for the optimality index measure, O, for each of the five seizure detection measures.

Table 3. Summary of performance of all the seizure detection measures: ED, embedding delay; WS, wavelet scale; HS, Hurst scale; NLA, nonlinear autocorrelation; VE, variance energy.

	Location	Ipsi-CA	Ipsi-DG	Contra-DG	Contra-CA
12K	ΔT	ED> WS	ED⩾ NLA⩾ WS	ED∼ WS	ED> WS⩾ NLA
	SK	WS⩾ NLA	WS⩾ NLA	NLA> WS	WS∼ NLA
	O	WS> NLA	NLA⩾ WS	WS⩾ NLA	WS∼ NLA> ED
200-I	ΔT	ED> WS∼ HS∼ VE	WS⩾ ED> NLA	WS∼ NLA∼ ED	ED> NLA∼ WS∼ VE
	SK	WS∼ VE	WS> NLA	VE> WS	WS> NLA⩾ VE
	O	WS⩾ VE	WS> ED	WS⩾ VE	WS> NLA
200-M	ΔT	ED⩾ WS			
	SK	VE⩾ ED			
	O	ED> WS⩾ NLA			

of-sample prospective approach. The authors suggest that future studies for seizure prediction should place emphasis sound methodology of EEG data acquisition and rigorous statistical validation. Early seizure detection algorithms on the other hand have recently provided some encouraging results [15, 16, 20] in terms of their ability to anticipate impending seizure with very high statistical robustness few seconds in advance of an overt clinical manifestation of the seizure. The critical parameter in the suitability of these algorithms is the time available between the detection of an impending seizure and the overt behavioral manifestation of the seizure. Our goal in this work was to determine whether the methodology of EEG data acquisition in terms of the type of recording electrodes (microwire electrodes versus

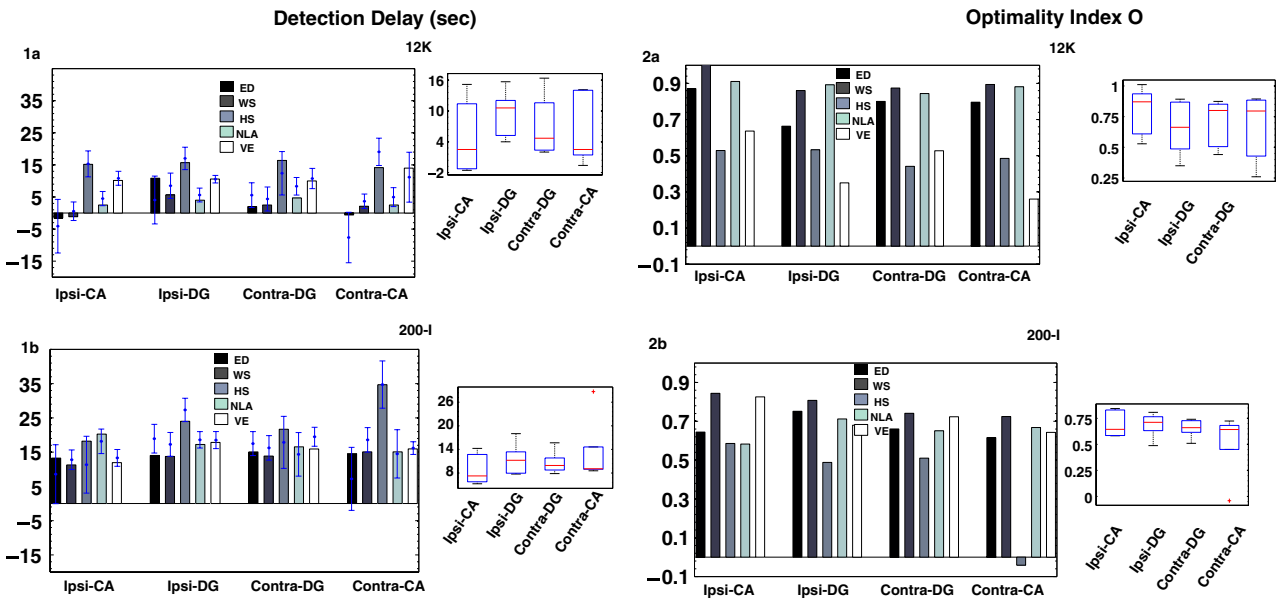

Figure 8. Comparison of the performance of the seizure detection measures, *M*, as a function of electrode placement for a given EEG sampling rate and a given electrode type. In figures 8-1(a) and (b), we compare the median delay in detection for each of the five seizure detection measures and the overall performance in terms of the location of the electrode placement for EEG acquisition (boxplot) for EEG sampling rates of 12 kHz and 200 Hz, respectively. In figures 8-2(a) and (b), a similar comparison is made for the optimality index measure, *O*, for each of the five seizure detection measures.

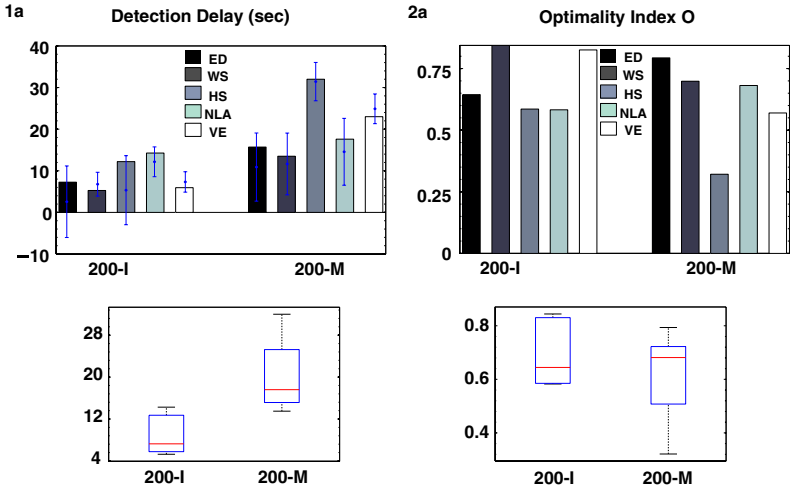

Figure 9. Comparison of the performance of the seizure detection measures *M*, dependent on the type of electrode used for EEG acquisition for given sampling rate of EEG acquisition. In figure 9-1(a), we compare the median delay in detection for each of the five seizure detection measures and the overall performance in terms of the type of electrode used for EEG data acquisition (boxplot) with microwire electrode array and stainless-steel screw electrodes respectively. In figures 9-2(a), a similar comparison is made for the optimality index measure, *O* for each of the five seizure detection measures.

stainless-steel screw electrodes), the sampling rate of the data acquisition (12 kHz versus 200 Hz) and the placement of the electrodes in the brain(ipsi-/contra-lateral dentate gyrus, CA regions) provide additional information about the seizure generation and thus improve the time of early seizure detection by a given seizure detection algorithm. We believe that information gained through this research would go a long way in making the optimal use of seizure detection algorithms in the development of a real-time seizure intervention system. With this goal in mind, in this paper we employed five well-known seizure detection algorithms in a rat model of temporal lobe epilepsy. Our aim was to study the performance of a subset of known non-parametric seizure detection algorithms to access their performance dependent on the method of EEG data acquisition. It was not our intention in this work to propose and analyze a new seizure detection algorithm. Two distinct performance criteria: (1) statistical robustness as determined through sensitivity and specificity for seizure detection, and

(2) the delay in detection of the seizure with respect to the electrographic seizure onset time were used to access the performance of each seizure detection algorithm studied. An empirical function, the optimality index O was defined in order to quantify the performance of all seizure detection measures, taking into account the two key performance criteria listed above. In summary, the main findings of this study were (1) early detection of spontaneous seizures in a rat model of temporal lobe epilepsy is feasible based on quantitative measures of the brain dynamics with very high statistical robustness; (2) each measure performed better in terms of high values obtained for the statistical measures for sensitivity and specificity to detect seizures. (3) The wavelet scale (WS) measure, outperformed all the other seizure detection measures considered in most configurations of the EEG acquisition with the highest optimality index value. This was in part due to the ability of WS to detect seizures very close to the EEG seizure onset time, which in turn, makes it most suitable as a method for a closed-loop seizure prevention system.

We began with showing an example of an EEG trace which demonstrates the complexity of the EEG structures and artifacts in the EEG data set acquired from long-term continuous recordings. We then presented examples of three morphological types of EEG seizures that are observed in the CLE rat model [3]. As can be seen from the corresponding time-frequency plots in figure 4, we observe a sustained increase in energy in the frequency band ≈0–50 Hz for entire duration of the seizure. Based on our observation that behavioral manifestation of the seizure typically occurs during the high amplitude EEG activity in the seizure epoch, we define the electrographic seizure onset time as the first time point in the EEG data when the amplitude of the EEG signal shows a sustained increase in amplitude. We then define the algorithmic seizure onset time as the time when a given seizure detection measure crosses a threshold T_M. The threshold T_M is optimized for each measure M dependent on the statistical parameters of the sensitivity and specificity of M to detect the EEG seizures. We then utilized an optimality index measure O that incorporates two key statistics, namely statistical robustness as measured by sensitivity and specificity to detect seizures and the mean delay in seizure detection, for evaluating the performance of all the early seizure detection algorithms considered in this work. The measure M were analyzed for performance based on the method of EEG acquisition. We observed that overall each measure M has better performance in terms of its ability to detect seizures for the EEG acquisition done at higher sampling rate of 12 kHz using microwire electrodes rather than the traditional approach of EEG data acquired at lower sampling rate of 200 Hz using a macrowire screw electrode. For the animal model of temporal lobe epilepsy considered in this work, we also observed that the overall performance is better for EEG data recorded from microwire electrodes located in the ipsi-/contra-lateral CA region, suggesting that the temporal initiation of the seizures is in the CA regions of the brain. Although the performance results with microwire electrode array at 200 Hz sampling rate are superior in comparison to the EEG data acquired with macrowire screw electrodes at the same sampling rate (figure 9), it remains to be seen whether this holds true for EEG data acquired at higher sampling rate using stainless-steel screw recording electrodes.

Previous animal studies have incorporated seizure prediction in models of provoked seizures. In *in vivo* studies, evidence of preictal transitions was reported for three-mercaptopropionic acid-induced seizures using stochastic methods [23], as well as for pentylenetetrazol-induced seizures using wavelet-based residual entropy [17]. Studies using brain slices in low [Mg^{2+}] solution have also reported prediction of seizure-like event in hippocampal networks using artificial neural networks [4, 5]. The use of a standard *in vivo* model of unprovoked seizures in the present study allowed a more direct comparison to the continuous data sets recorded from humans with epilepsy undergoing pre-surgical evaluation. Compared to the spontaneous seizures recorded in the rat model of temporal lobe epilepsy, typical human data sets include fewer seizures, with higher variability and too few interictal data set for reliable estimation of false warnings. Use of an animal model of spontaneous limbic seizures under controlled experimental conditions can therefore provide numerous insights into the interpretation of human data that can be confounded due to differences in seizure etiology (i.e., tumor, stroke, infection, trauma), lesion type and location, and effects of anti-epileptic drug use. In addition the animal model gives us an added advantage to study the pre-clinical performance of a given seizure detection measure, dependent on the method of EEG data acquisition.

In summary the enhancement in the performance of several seizure detection methods presented here dependent on more refined data acquisition techniques (high sampling with microwire electrode arrays) warrant further testing with more sophisticated refinement of the seizure detection methods. Continued use of the rat model of temporal lobe epilepsy can provide pre-clinical controlled experimental conditions to enable further testing and systematic improvement in early seizure detection software. Ultimately, these studies are intended to translate into the development of implantable closed-loop control systems capable of activating physiological or pharmacological interventions to prevent impending seizures in patients with intractable epilepsy.

Acknowledgments

This research was supported by the National Institutes of Biomedical Imaging and Bioengineering (NIBIB) through Collaborative Research in Computational Neuroscience (CRCNS) grant number R01NS050582-01A1, Bioengineering Research Partnership Grant Number R01EB002089, the Wilder Center of Excellence for Epilepsy Research and the Children's Miracle Network. SST was partially funded through the fellowship grant from the Epilepsy Foundation of America. PRC was partially funded through the BJ and Eve Wilder endowment funds. WLD was partially supported through the J Crayton Pruitt Family Endowment funds. The analysis work in this project was sponsored through grant from the office of Naval research (grant number N00014-02-1-1019) and the fellowship from the Epilepsy Foundation of

America for SST . We would like to thank the lab technician Morgan Guoan who performed all the surgeries for electrode implantations and Dr Wendy Norman who provided her kind assistance in scanning the EEG/video data to identify the seizures and creating the control data sets for the statistical analysis.

References

[1] Abarbanel H D I 1996 *Analysis of Observed Chaotic Data* (New York: Springer)
[2] Bassingthwaighte J B, Liebovitch L S and West B J 1994 *Fractal Physiology* (Oxford: Oxford University Press)
[3] Bertram E H 1997 Functional anatomy of spontaneous seizures in rat model of limbic epilepsy *Epilepsia* **38** 95–105
[4] Chiu A W, Daniel S, Khosravani H, Carlen P L and Bardakjian B L 2005 Prediction of seizure onset in an *in-vitro* hippocampal slice model of epilepsy using Gaussian-based and wavelet based artificial neural networks *Ann. Biomed. Eng.* **33** 798–810
[5] Chiu A W, Kang E F, Derchansky M, Carlen P L and Bardakjian B L 2006 Online prediction of onsets of seizure-like events in hippocampal neural networks using wavelet artificial neural networks *Ann. Biomed. Eng.* **34** 282–94
[6] Elger C E and Lehnertz K 2000 Seizure prediction by nonlinear time series analysis of brain electrical activity *Eur. J. Neurosci.* **12** 2124–34
[7] Iasemidis L D, Pardalos P M, Sackellares J C and Shiau D S 2001 Quadratic binary programming and dynamical systems approach to determine the predictability of epileptic seizures *J. Comb. Optim.* **5** 9–26
[8] Iasemidis L D, Shiau D S, Chaovalitwongse W, Sackellares J C, Pardalos P M, Principe J C, Carney P R, Prasad A, Veeramani B and Tsakalis K 2003 Adaptive epileptic seizure prediction system *IEEE Trans. Biomed. Eng.* **50** 616–27
[9] Iasemidis L D, Shiau D S, Sackellares J C, Pardalos P M and Prasad A 2004 Dynamical resetting of the human brain at epileptic seizures: application of nonlinear dynamics and global optimization techniques *IEEE Trans. Biomed. Eng.* **51** 493–506
[10] Latka M, Was Z, Kozik A and West B 2003 Wavelet analysis of epileptic spikes *Phys. Rev.* E **667** 052902
[11] Lehnertz K and Elger C E 1998 Can epileptic seizures be predicted? *Phys. Rev. Lett.* **80** 5019–22
[12] Litt B *et al* 2001 Epileptic seizures may begin hours in advance of clinical onset: a report of five patients *Neuron* **30** 51–64
[13] Mormann F, Andrzejak R G, Elger C E and Lehnertz K 2003 Automated detection of a preseizure state based on a decrease in synchronization in intracranial electroencephalogram recordings from epilepsy patients *Phys. Rev.* E **67** 021912-1–10
[14] Mormann F, Andrzejak R G, Elger C E and Lehnertz K 2007 Seizure prediction: the long and winding road *Brain* **130** 314–33
[15] Osorio I, Frei M G, Sunderam S, Giftakis J, Bhavaraju N C, Schaffner S F and Wilkinson S B 2005 Automated seizure abatement in humans using electrical stimulation *Ann. Neurol.* **57** 258–68
[16] Osorio I, Frei M G and Wilkinson S B 1998 Real-time automated detection and quantitative analysis of seizures and short term prediction of seizure onset *Epilepsia* **39** 615–27
[17] Paul J S, Patel C B, Al-Nashash H, Zang N, Ziai W C, Mirski M A and Sherman D L 2003 Prediction of PTZ-induced seizures using wavelet-based residual entropy of cortical and subcortical field potentials *IEEE Trans. Biomed. Eng.* **50** 640–8
[18] Qu H and Gotman J 1993 Improvement in seizure detection performance by automatic adaptation to the EEG of each patient *Clin. Neurophysiol.* **86** 79–87
[19] Le Van Quyen M, Martinerie J and Navarro V 2001 Anticipation of epileptic seizures from standard EEG recordings *Lancet* **357** 183–8
[20] Saab M E and Gotman J 2005 A system to detect the onset of epileptic seizures in scalp EEG *Clin. Neurophysiol.* **116** 427–42
[21] Sanchez J C, Mareci T, Norman W M, Principe J, Ditto W and Carney P R 2006 Evolving into epilepsy: multiscale electrophysiological analysis and imaging in an animal model *Exp. Neurol.* **198** 31–47
[22] Shin C and McNamara J O 1994 Mechanism of epilepsy *Ann. Rev. Med.* **45** 379–89
[23] Sunderam S, Osorio I, Frei M G and Watkins J F 2001 Stochastic modeling and prediction of experimental seizures in Sprague-Dawley rats *J. Clin. Neurophysiol.* **118** 275–82
[24] Talathi S S, Hwang D U, Ditto W and Carney P R 2007 Early seizure detection in animal model of temporal lobe epilepsy *Data Mining, Systems Analysis and Optimization in Biomedicine* ed O Seref and P M Pardalos *AIP Conf. Proc.* **953** 292–307
[25] White A M, Williams P A, Ferraro D J, Clark S, Kadam S D, Dudek F E and Staley K J 2006 Efficient unsupervised algorithms for the detection of seizures in continuous EEG recordings from rats after brain injury *J. Neurosci. Methods* **152** 255–66
[26] Xiaoli L, Polygiannakis J, Kapiris P, Peratzakis A and Eftaxias K 2005 Fractal spectral analysis of pre-epileptic seizures in terms of criticality *J. Neural. Eng.* **2** 11–6